2016-01-0856

The Effects of Injection Timing and Duration on Jet Penetration and Mixing in Multiple-Injection Schedules

Author, co-author (Do NOT enter this information. It will be pulled from participant tab in MyTechZone)

Affiliation (Do NOT enter this information. It will be d from participant tab in MyTechZone)

Abstract

Advanced injection schedules involving multiple injections have been utilized for reducing the peak cylinder pressure, phasing heat release rate, and reducing emissions in diesel engines. The timing and duration of the injections determine the injection schedule efficacy at achieving these effects. The goal of this work is to develop tools to track multiple injections to develop a better understanding of interaction mechanisms between subsequent injections. Both timing and duration effects are captured by using three different dwell times and seven injection durations. Experimental gas jet studies are conducted using schlieren. The jet-tip penetration rate, *S*, results do not reveal significant differences in jet-tip penetration with variations in the first-injection duration and dwell between injections. However, it was found that the jet spreading angles between the first and second injections differed, with the first injection having a higher average angle during the quasi-steady portion of the injection. This is indicative of differences in jet mixing and entrainment between the first and second injection.

Introduction

Exhaust emissions from diesel engines contain numerous pollutants including particulate matter (PM), nitrogen oxides (NO_x), and unburned hydrocarbons (UHC); the released quantities of these emissions are limited by emissions regulations [1, 2]. Aftertreatment techniques, such as diesel particulate filters (DPF) and selective catalytic reduction (SCR), have proven to be effective in reducing PM and/or NO_x emissions. However, aftertreatment systems are often costly to install and reduce efficiency by adding weight to the vehicle, which motivates research to improve upon in-cylinder emissions reduction methods such as advanced injection timing.

The multiple-injection schedules considered in this work divide a quantity of injected fluid into two consecutive injections (i.e. pilot, split, and post injections). Multiple injection schemes have been utilized in practice to alter the heat release rate (HRR), peak cylinder pressure, and combustion emissions. The terminology used for subsets of multiple injections is based on the quantity of fuel that is used during different portions of the schedule. The injection that uses the most fuel is considered the main injection. When shorter injections precede the main injection, the short injections are referred to as the pilot injections. When the shorter injections are subsequent to the main injection, the shorter injection is called a post injection. An injection schedule with two equal injections will be referred to as a split injection in this paper.

Pilot injections have been effective in reducing the peak cylinder pressure and combustion noise level (CNL) [3-5]. Combustion phasing reduces HRR and the peak cylinder pressure, effectually reducing engine noise and decreasing the stress on engine components. Busch *et al.* [5] showed that close-coupled pilot injections (dwell of 140 μs) reduced the CNL under part-load operating conditions by roughly 9 dB compared to a single injection without increasing soot, NO_x, CO, or UHC emissions. In addition to CNL reduction, Tanaka *et al.* [3] showed that pilot injections can simultaneously decrease PM and NO_x emissions. The timing of pilot injections in relation to the main injection (changing dwell) has been used to change the combustion duration. Zeng *et al.* [6] used pilot injections with the same injected mass quantity and same duration of injection (DOI) but different dwell times to show that advanced pilot injection timing (30 degrees BTDC) decreased the HRR, decreased combustion duration, and produced the lowest in-cylinder soot levels within their test matrix.

Split injections have been used primarily in injection studies, rather than practical application, to understand the effects of altering dwell time between injections alone [7-13]. A split injection schedule is currently the focus of one of the Engine Combustion Network (ECN) spray cases (Spray A) [14, 15]. Herfatmanesh *et al.* [13] compared the quantities of soot, NO_x, and UHCs produced by single injections and split injections; the results showed that the split injections did not decrease emissions and rather significantly increased soot production. However, other authors [7, 9-12] showed that split injections did decrease NO_x emissions but only with certain dwell times. Goldwine and Sher [16] compared schedules with two different pilot injections with a split injection schedule across a range of dwell times. Their results showed that the split injection schedule produced the highest NO_x emissions but the lowest CO emissions across all dwell times and the lowest UHC emissions at long dwell times [16]. There is a tradeoff in decreasing the CO and UHC emissions using split injections, whereby NO_x emissions increase (and vice versa).

Close-coupled post injections have been utilized to decrease UHC and soot emissions. Herfatmanesh and Zhao [17] showed that a post-injection strategy used in place of a single injection with the same total injected fuel quantity can result in significantly lower UHC emissions, improved mixing, better fuel evaporation, and lower CNL. O'Connor and Musculus [18] showed a 34% reduction in UHC

emissions as compared to a single injection case at the same load using close-coupled post injections in a heavy-duty diesel engine with EGR. Once again, there is an emissions tradeoff and reducing UHC by using a split injection results in an increase in NO_x emissions [17]. Numerous studies have shown that post injections can be used to reduce engine-out soot [19-26] .

This brief review of the literature highlights the numerous benefits of properly timed multiple-injection schemes with regards to CNL and emissions, and provides insight into some of the offsetting weaknesses. Multiple-injection strategies in diesel engines are already used for engine performance optimization. However, these methods are typically optimized on a case-by-case basis through an extensive series of tests. An understanding of the mechanisms of injection interactions would enable optimal combustion conditions to be determined more efficiently. The objective of this work is to explore the fluid mechanic interactions between multiple consecutive injections in free jets.

There are several physical effects of multiple injections that have been previously studied. Slipstreaming is a phenomenon that occurs when the penetration rate of a subsequent injection in a multiple-injection scheme is higher than it would be if that injection were penetrating into a quiescent media. In a study by Skeen *et al.* [14], this effect was seen using schlieren measurements, which showed that the second injection had entered a "slipstream" produced by the first injection wherein the fluid ahead of the second injection was already moving downstream after SOI_2. However, the first jet was injected into stagnant fluid, which resulted in a stagnation plane at the head of the jet. A fundamental study of liquid and vapor penetration of injections under engine-like conditions showed similar findings [27]. The split-injection case showed that the liquid penetration of the second injection was higher than the penetration of the first injection for the two shortest dwell times. Those results indicate that jet-tip penetration is a function of both DOI_1 and the residual flow field from the first injection [27]. Slipstreaming is investigated as a function of DOI_1 and dwell time using penetration measurements from schlieren imaging in this study.

Mixing is a second fluid-mechanic phenomenon that affects combustion processes and changes with injection duration and timing. Here, we focus on the mixing of fluid from two consecutive injections. Previously, Bruneaux and Maligne [28] compared tracer laser-induced exiplex fluorescence (LIEF) measurements for single injections and main plus post injections to determine the effects of injection timing and dwell on mixing. Their results showed that entrainment after the end of injection (EOI) resulted in low fuel concentrations near the tail of the jet. High concentrations at the jet tip were caused by limited mixing near the head of the jet. In the post-injection cases, the second injection followed a similar trend to the first injection. However, the OH-concentration gradient at the tip of the jet was less steep than it was in the first injection, indicating increased mixing in the jet-tip region. Comparisons of the post injections for two different dwell times showed that the gradient at the tip of the jet was steeper when the dwell time was longer, which implies that more mixing occurs at the head of the post injection jet when the dwell time is shorter [28]. Mixing will be investigated using the dispersion angle of the jet, which is measured from schlieren images.

In this study schlieren imaging in a helium gas jet is used to capture the jet-tip penetration and dispersion angle and to explain fluid mechanic interactions across a range of multiple-injection schemes. Helium was chosen as the working fluid because it has a lower density than air, which allows it to be seen using the schlieren technique by showing variations in the refractive index due to density gradients. Helium also can be safely exhausted into the laboratory air. Measurements taken in engine and spray vessel experiments often do not capture detailed fluid mechanics due to limitations in optical access and difficulty in seeding the flow, though recent experiments have shown more success using these techniques [29-32]. Gas jet experiments are an alternative means by which key physical phenomena may be measured; gas jets have been shown to capture penetration and entrainment rates of vaporizing and non-vaporizing sprays [33-35]. For example, fundamental gas jet experiments by Abani and Ghandhi [34] demonstrated important physics about injection ramp rates and showed strong parallels with diesel fuel injection. Additionally, Naber and Siebers [33] have shown that the characteristics of diesel sprays can be inferred from gas jet results by non-dimensionalizing experimental gas jet conditions and scaling to diesel conditions.

Naber and Siebers [33] showed that ambient gas density has a large effect on jet-tip penetration and their scaling equations account for that effect as well as the gas/fuel density and injector geometry. The scaling equations for the penetration length (x^+) and time (t^+) are given in Equation 1 and Equation 2, respectively [33].

$$x^+ = \frac{d_f \cdot \sqrt{\tilde{\rho}}}{a \cdot \tan(\theta/2)} \quad (1)$$

$$t^+ = \frac{d_f \cdot \sqrt{\tilde{\rho}}}{a \cdot \tan(\theta/2) \cdot U_f} \quad (2)$$

The angle θ is the dispersion angle of the spray, the term a is equivalent to 0.66 and is used to relate the tangent of the measured spray angle to the spray dispersion angle. The effective diameter (d_f) of the gas exiting the injector orifice is approximately 0.8 for this experiment and was calculated using Equation 3 [33], while the actual diameter of the orifice (d_o) is 1 mm. C_a is the area contraction coefficient, which is roughly 0.6 for a sharp-edged circular orifice.

$$d_f = \sqrt{C_a} \cdot d_o \quad (3)$$

The fuel density ratio ($\tilde{\rho}$), given in Equation 4 [33], is the ratio of the fuel density (ρ_f) to the ambient density (ρ_a).

$$\tilde{\rho} = \rho_f / \rho_a \quad (4)$$

A measurement of the velocity of the jet as it exits the orifice was attempted using PIV, but we were unable to resolve the exit velocity with the PIV algorithm. Therefore, the velocity (U_f) of the gas jet as it exits the orifice is calculated using Equation 5 [33], where the flow coefficient is C_v, the injection pressure of the fuel is P_f and the ambient pressure in the laboratory is P_a.

$$U_f = C_v \cdot \sqrt{2 \frac{(P_f - P_a)}{P_f}} \quad (5)$$

The dimensionless penetration time and dimensionless penetration distance are given in Equation 6 and Equation 7, respectively, where t is the actual time and S is the measured penetration distance [33].

$$\tilde{t} = t/t^+ \quad (6)$$

$$\tilde{S} = S/x^{+} \quad (7)$$

The dimensionless penetration and time calculated from Equation 6 and Equation 7 will be used to discuss the results, which will enable easy comparison with vaporizing spray results from other studies. PIV results be used in future work to understand both the jet momentum and entrainment. The concentration of injected fluid will be determined using acetone tracer-PLIF, which provides an indication of the expected equivalence ratio, ϕ, in regions of the jet during fuel injections. The techniques discussed in this work can be applied to both Mie-scattering and tracer-PLIF to better quantify turbulent mixing in these systems.

Experimental Overview

Experimental Setup

The experimental setup for the gas jet experiments is shown in Figure 1 and follows that of Abani and Ghandhi [34]. The gas from the supply canisters is fed into a single injector through two fast-acting valves. A pressure transducer is located on the side of the injector to monitor the pressure in the injector, and a relief valve allows for fast ramp down times. The pressure recorded by the pressure transducer is used to generate the injection pressure profiles presented in the *Results* section.

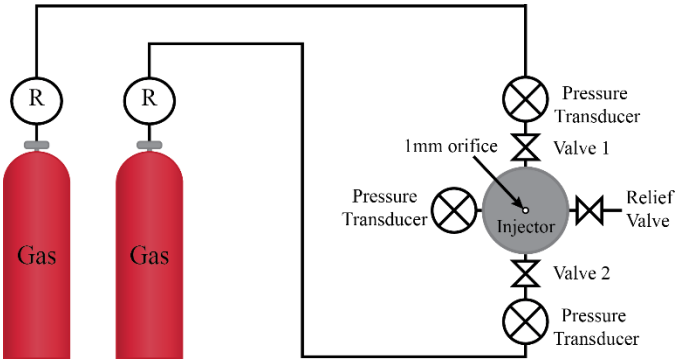

Figure 1. Experimental setup for gas jet experiments showing two helium tanks with regulators (R), three pressure transducers, three valves, and the injector.

The gas jet is produced from a 1 mm orifice in the center of the ¼ inch thick plate into quiescent air at ambient temperature and pressure. A top-view cross-section of the injector cavity is shown in Figure 2.

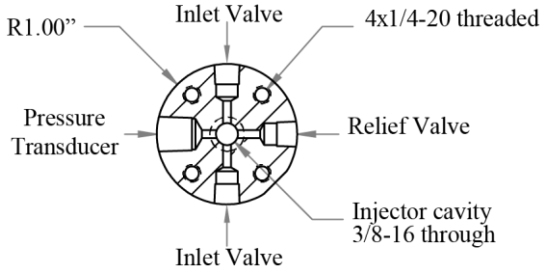

Figure 2. The cross-sectional cut of the injector body shows the 1/8" tapped holes for the two-way fast acting valves that feed air into the chamber and the relief valve as well as the 1/4" NPT hole for the pressure transducer.

Diagnostics and Controls

A z-type schlieren configuration is used to visualize the gas jet for determining jet-tip penetration and dispersion angle. Light is provided by a continuous LED, and 6" parabolic mirrors are used on either side of the setup. High-speed images are captured with a Photron SA1.1 Fastcam. The camera has a viewing region that is 384 by 864 pixels. The maximum height and width of the images are 12.5 cm and 5.8 cm, respectively, providing a resolution of 65.5 pixels/cm. The images are recorded at 15000 fps.

Jet penetration and dispersion angle are calculated from the ensemble average of 20 repetitions of each experiment; previous experimentation showed that injection pressure statistics converged after 15 ensembles. Each set of images is first background subtracted, median filtered, then binarized at each instant in time. The binarized images are ensemble averaged and binarized a second time. This process reduces image noise and increases the accuracy of jet penetration and dispersion angle measurements. Calculating the jet-tip penetration of the second injection in each set requires a sliding background subtraction step to locate the jet tip on a background that still contains signal from the first injection. Processing the gas jet images for the second injection is a nontrivial process and is described in detail in Appendix A.

A National Instruments data acquisition system (DAQ) and LabView software are used to control valve timing, record pressure data, and trigger the camera. The injection chamber pressure is recorded at a rate of 45000 Hz.

Injection Schedules

The test matrix for this study, shown in Table 1, includes injection schemes with two injections of varying duration and three different dwell times. A single injection with a DOI that is the same as the total injection time for the multiple-injection cases is used for comparison. The non-dimensional injection durations are of the same order of magnitude of many fuel injections, and were chosen to optimize the clarity of the experimental results.

This test matrix allows effects of the relative duration and dwell between the first and second injection to be investigated. Variations in dwell time are expected to affect the extent of slipstreaming and the dispersion of the first injection prior to SOI_2. The dispersion of the first injection subsequently affects the amount of entrainment of the fluid from the first injection into the second injection. In an engine, the velocity of the second injection relative to the first injection and the entrainment of first injection fluid into the second injection would affect the local mixture composition.

The relative duration of the injections also influences the physics of the interaction. The flow field and local mixtures that result from a main injection interacting with a short pilot injection are different than for a short post injection interacting with a main injection. It is expected that pilot and post injections of varying durations will behave differently. The test schedule is devised to include pilot, split and post injections. For each of the three dwell times ($\tilde{t} = 211.1$, 422.1, and 633.2) there are seven first- and second-injection timings, which sum to a total $\tilde{t} = 2532.6$ (60 ms) injection duration.

Table 1. The injection strategies included pilot, split, and post injections with three different dwell durations given in non-dimensional time ($\tilde{t}$): short 211.1 (5 ms) dwell (cases 1 – 7), intermediate 422.1 (10 ms) dwell (cases 8 – 14), and long 633.2 (15 ms) dwell (cases 15 – 21). The multiple injections were compared with a 2532.6 (60 ms) single injection (case 22).

Case #	Peak Chamber Pressure	1st Injection Duration	Dwell	2nd Injection Duration
1	100	633.2	211.1	1899.5
2	100	844.2	211.1	1688.4
3	100	1055.3	211.1	1477.4
4	100	1266.3	211.1	1266.3
5	100	1477.4	211.1	1055.3
6	100	1688.4	211.1	844.2
7	100	1899.5	211.1	633.2
8	100	633.2	422.1	1899.5
9	100	844.2	422.1	1688.4
10	100	1055.3	422.1	1477.4
11	100	1266.3	422.1	1266.3
12	100	1477.4	422.1	1055.3
13	100	1688.4	422.1	844.2
14	100	1899.5	422.1	633.2
15	100	633.2	633.2	1899.5
16	100	844.2	633.2	1688.4
17	100	1055.3	633.2	1477.4
18	100	1266.3	633.2	1266.3
19	100	1477.4	633.2	1055.3
20	100	1688.4	633.2	844.2
21	100	1899.5	633.2	633.2
22	100	2532.6	N/A	N/A

There are nine pilot injection cases (1, 2, 3, 8, 9, 10, 15, 16, and 17), three split injection cases (4, 11, and 18), nine post injection cases (5, 6, 7, 12, 13, 14, 19, 20 and 21), and a single injection case (22) in total. The split injection cases are of particular interest because a multiple-injection case consisting of equal split injections (Spray A) is currently a focus of the Engine Combustion Network (ECN) [15].

Results and Discussion

Single Injection Baseline

A single 2532.6 non-dimensional injection time, $\tilde{t}$, (60 ms in real time) is used for case 22 for baseline comparisons for the 21 multiple-injection cases in Table 1. The pressure profile for the single injection case, given in Figure 3, shows that the pressure peaked at 107.5 kPa and the actual non-dimensional DOI was 2583.3. The experimental setup provides highly repeatable injections, as shown in Figure 3, which shows +/- one standard deviation for the ensemble averaged pressure profile.

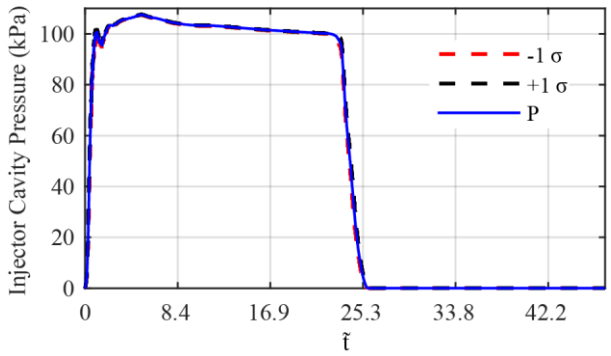

Figure 3. The pressure profile for the 2583.3 (61.2 ms) single injection case +/- 1 standard deviation for 20 ensemble averaged trials shows that the gas jet experiments were highly repeatable.

To quantify the ramp rates and ensure that the different injection cases have nearly the same ramp-up rate, a sixth order polynomial curve is fit to the ramp up portion of the pressure curves ($\tilde{t}$ = 0 to 1.27) for each case. The instantaneous ramp rate is calculated as the derivative of the polynomial function at each point in time. The polynomial fit of the ramp-up portion of the single injection and the instantaneous ramp rate are shown in Figure 4 as an example of the calculation.

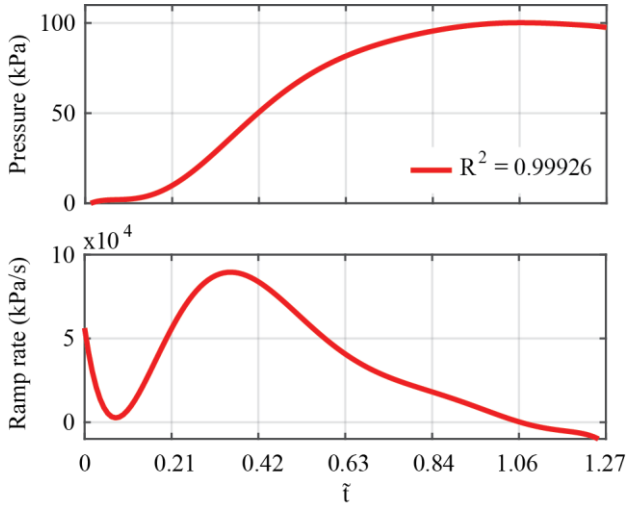

Figure 4. The sixth order polynomial fit of the first $\tilde{t}$ = 1.27 (3 ms) of the single injection pressure curve (top) was used to calculate the instantaneous ramp rate (bottom) by taking the derivative of the polynomial function.

Pressure Traces

The injection pressure profiles presented in this section are ensemble averaged for 20 ensembles of the same injection timing. The pressure profiles for pilot, split, and post injection cases with varying dwell times but the same injection durations are given in Figure 5, Figure 6, and Figure 7, respectively. Injections with the same dwell time but different injection durations are also compared. A lower peak injection pressure during the second injection is an overall trend in all of the test cases.

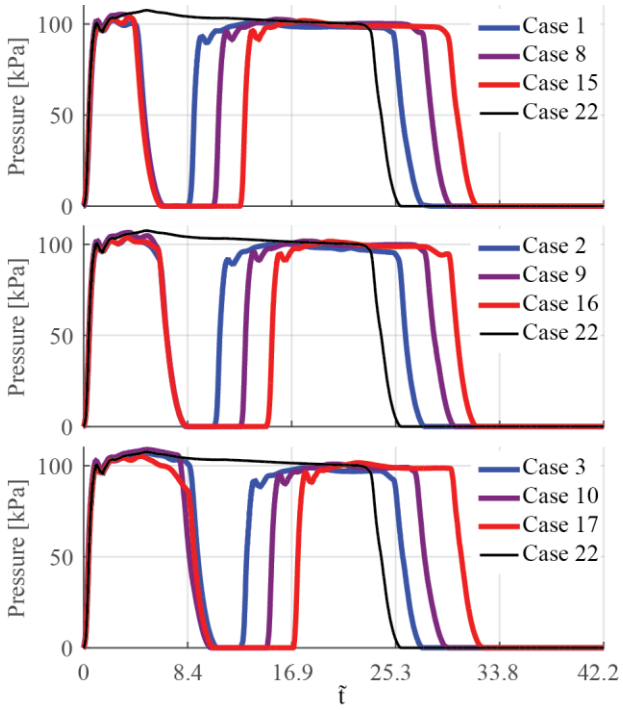

Figure 5. The pressure profiles for pilot injections with similar injection durations but different dwell times are compared with the baseline case and shown for (top) cases 1, 8, and 15, (center) cases 2, 9, and 16, and cases (bottom) 3, 10, and 17.

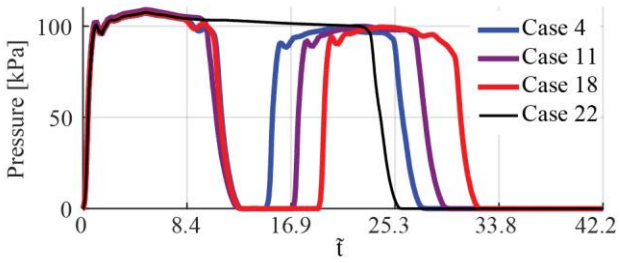

Figure 6. The pressure profiles for split injections with similar injection durations but different dwell times are compared with the baseline case.

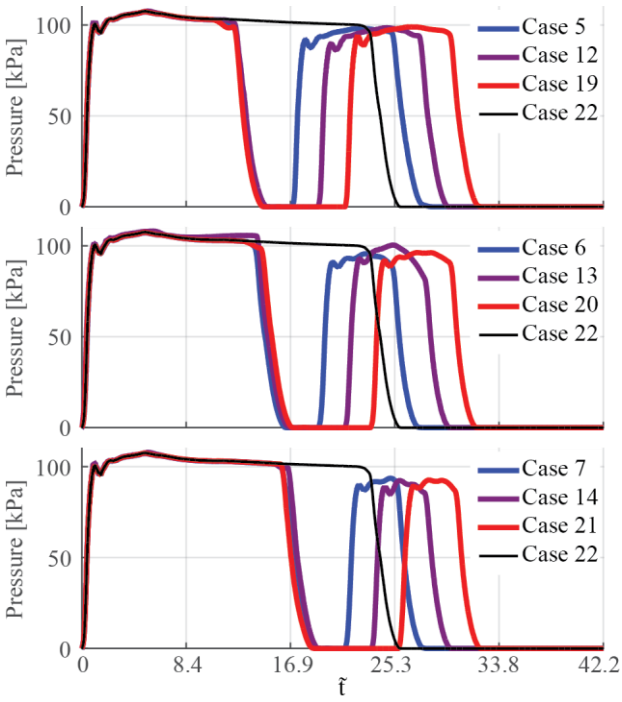

Figure 7. The pressure curves for post injections with similar injection durations but different dwell times are compared with case 22 and shown for (top) cases 5, 12, and 19, (center) cases 6, 13, and 20, and (bottom) cases 7, 14, and 21.

Jet-tip Penetration

The jet-tip penetration, *S*, is determined by tracking the tip of the helium gas jets in the schlieren images. The viewing window has a height of 12.5 cm, limiting the distance over which the jet-tip penetration is measured. The penetration rate of the first injection is determined for each trial and averaged over 20 ensembles. To enhance image processing, ensemble averaged images are used to track the jet-tip penetration of the second injection. Therefore, the standard deviation of S_2 is not provided but is expected to be similar to that of S_1.

Comparisons of S_1 and S_2 across all multiple-injection cases show that there is not a significant difference in the jet-tip penetration up to 12.5 cm downstream of the injector. Figure 8 and Figure 10 show the jet-tip penetration for pilot injections and post injections, respectively, with the same injection durations but varying dwell time. Figure 9 shows the jet-tip penetration for the split injections.

The slipstreaming phenomenon that was previously noted in other experimental work on multiple injections was not observed in the results of this study. While slipstreaming was not observed under these test conditions, previous pilot injection tests with this injector did result in a higher jet-tip penetration for the second injection near EOI.

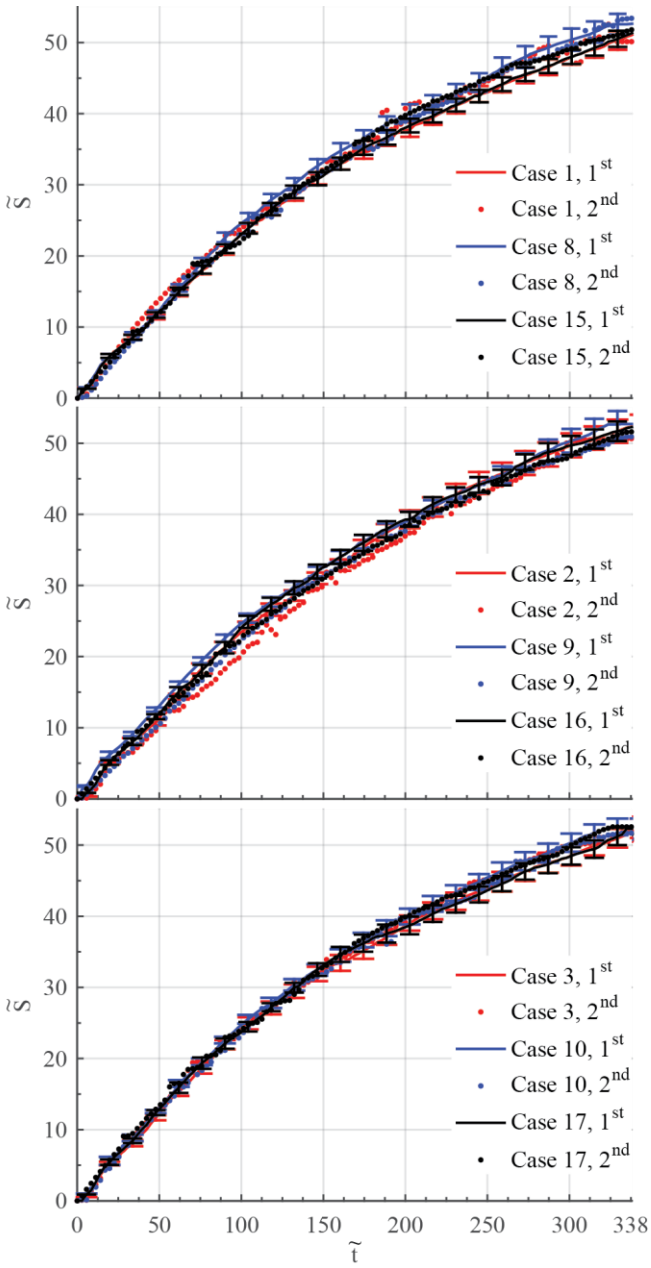

Figure 8. The jet-tip penetration of the first injection (S_1) and the jet-tip penetration of the second injection (S_2) are shown for pilot injections with different dwell periods. There is not a significant difference in S_1 and S_2.

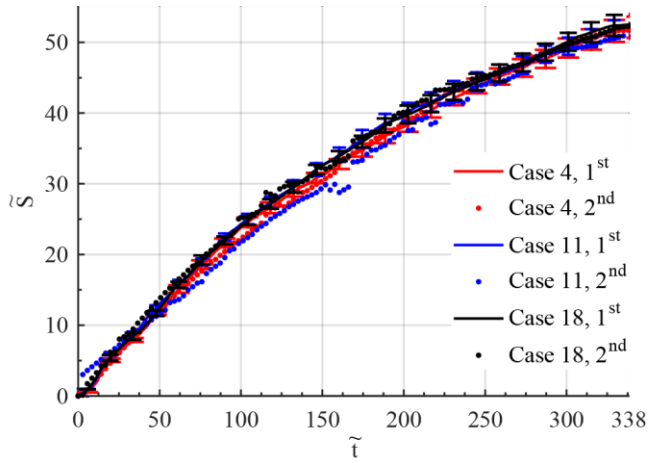

Figure 9. S_1 and S_2 are shown for split injections with different dwell times.

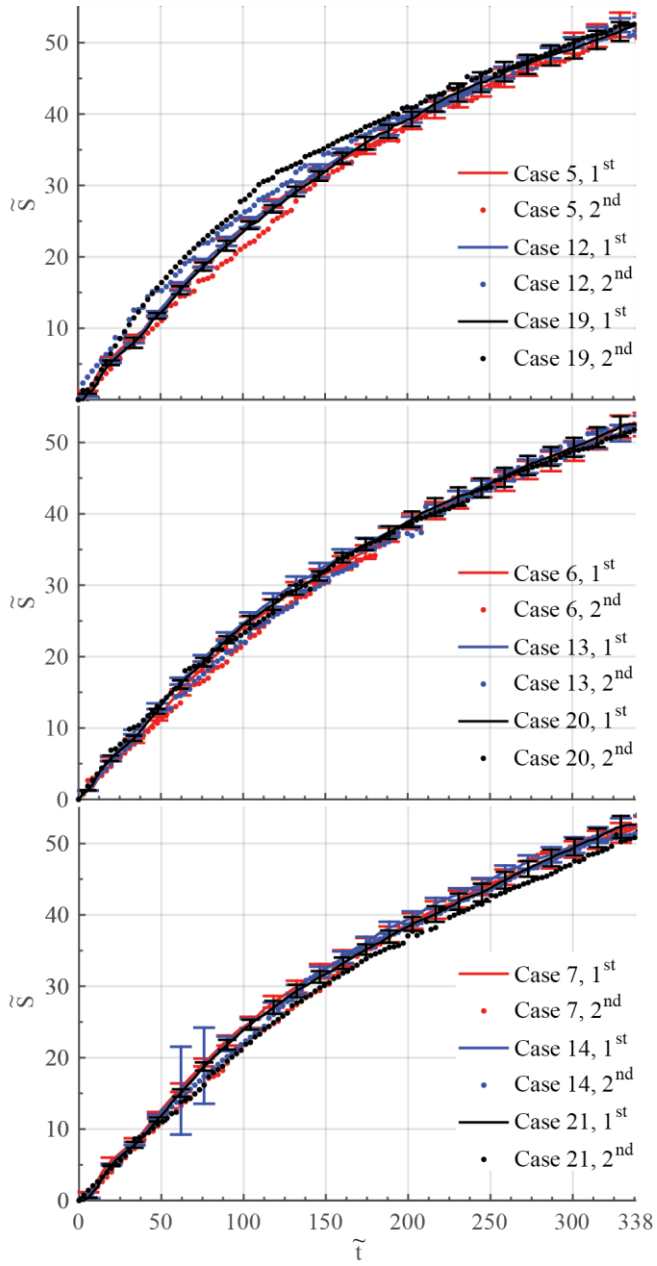

Figure 10. S_1 and S_2 are shown for post injections with different dwell times.

Dispersion Angle

The jet dispersion angle, θ, is a metric that correlates with the amount of fluid entrained into a jet [36]. Previous studies on non-vaporizing sprays have shown that the dispersion angle depends on the ambient density [37]. Because the second gas jet is injected into air mixed with helium from the first injection, the ambient density is lower during the second injection than during the first injection. Additionally, the ambient turbulence level increases after the end of the first injection. Therefore, it is expected that the dispersion angle of the first and second injections will not be the same. A difference in dispersion angle implies that the entrainment of air into the gas jet and the extent of mixing are different during the first and second injections.

At the beginning of an injection, the jet dispersion angle is high and decreases with time until it becomes nearly constant [31, 33]; this phenomenon was observed in the instantaneous dispersion angle results as shown in Figure 11 for a split injection (case 11).

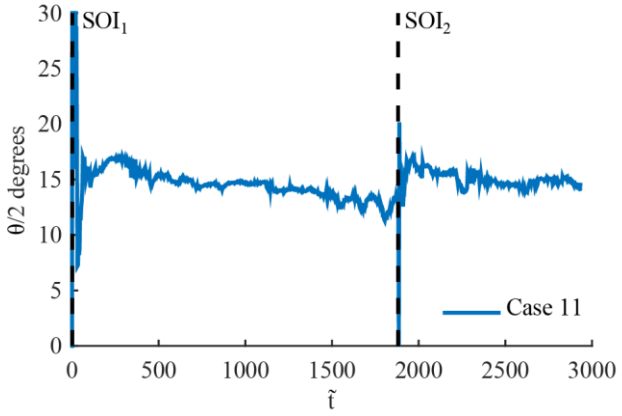

Figure 11. The half angle, $\theta_1/2$ and $\theta_2/2$, is given at each instant in time for both the first and second injection for the $\tilde{t}$ = 422.1 dwell split-injection case. The black dashed lines indicate SOI_1 and SOI_2.

Generally, the first injection has a higher half angle than the second injection, as shown for the split injection cases in Figure 12. With the exception of cases 17 and 19, any cases where $\theta_2/2$ was less than $\theta_1/2$ the half angle for the second injection was within +/- one standard deviation of the dispersion angle of the first injection.

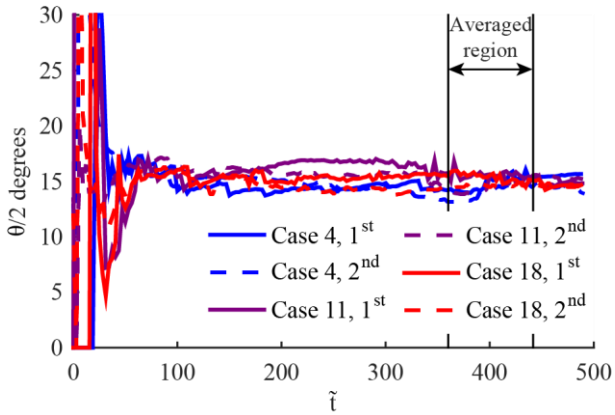

Figure 12. The half angle, $\theta_1/2$ and $\theta_2/2$, are given in relative non-dimensional time from SOI_1 and SOI_2 for both the first and second injection for the $\tilde{t}$ = 422.1 dwell split-injection case.

To compare the average dispersion angle during the quasi-steady portion of the injection across test cases, the half angle was averaged over 30 frames that represent the same time from SOI for each injection, as shown in Figure 12. The average half angle for the first and second injections are 15.4 degrees and 15 degrees, respectively. The error bars on the data indicate the 95% confidence interval for each averaged angle. Comparisons across different dwell times and injection durations show that injection angle does not vary with the duration of injection nor dwell time. It is apparent, however, that θ_1 is generally higher than θ_2, as shown in Figure 13.

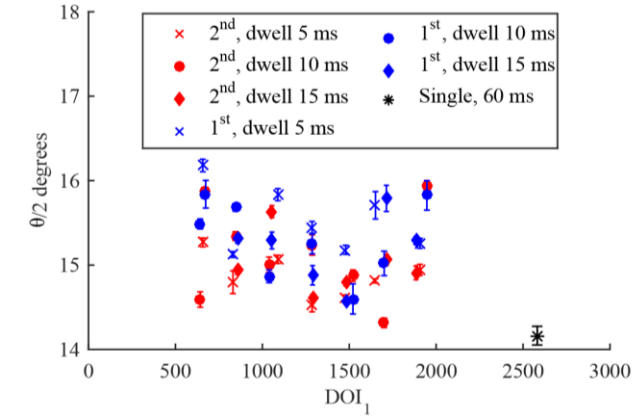

Figure 13. The averaged dispersion half angle, θ/2, is shown as a function of first injection time for various dwell periods. There does not appear to be a trend with dwell time nor injection duration. The error bars show the confidence interval. The average confidence interval for θ_1 and θ_2 are 0.10 and 0.07, respectively. Note: the limits of the y-axis are 14 to 18 degrees.

Differences in the dispersion angle are also observed by looking at the ensemble-averaged schlieren images, as shown in Figure 14. Following Skeen *et al.* [14], the first injection is shown by the red outline, while the ensemble-averaged inverted schlieren image shows the second injection. Figure 14 shows the three split-injection cases at various instances in time. At $\tilde{t}$ = 168.84 after SOI, the second injection dispersion angle is visibly less than the dispersion angle of the first injection.

Summary/Conclusions

This study describes the behavior of multiple-injection strategies in a gas jet system designed to mimic the behavior of diesel injection. Systematic variations in the injection schedule are designed to understand the impact of the duration of the first injection and the dwell between injections on the penetration rate and dispersion angle of the second injection. Analysis of high-speed schlieren imaging shows that the penetration rate of the second injection in the near-nozzle region is unaffected by changes in DOI_1 and the dwell between injections. Comparisons of the dispersion angles between the first and second injection show that the first injection has a higher dispersion angle than the second injection.

These penetration rate and dispersion angle results are critical to understanding key injection and mixing processes seen in multiple-injection scenarios. In particular, we have shown that in the near-nozzle region, the presence of a first injection does not affect the penetration of the head of the second injection, meaning that the slipstreaming effect may only be felt further downstream. In the near-nozzle region, the jet momentum is likely dominated by the injector pressure driving the injector rather than the injected fluid. However, further downstream, the slipstreaming effect may play a

larger role as the momentum of the jet is determined by both the jet fluid as well as the entrained fluid. Additionally, the density differences between helium and air versus those between vaporized diesel fuel and air will change both the momentum of the jets as well as the density of the surroundings.

Differences in the jet spreading angles between the first and second injections may indicate a difference in the mixing processes in the near-nozzle region between the first and second injection. These near-nozzle mixing processes determine important quantities in a reacting jet, including ignition delay time, lift-off length, and soot volume fraction in the spray. Further investigations using high-speed laser-induced fluorescence will be used to better understand these near-nozzle mixing processes during multiple-injection strategies.

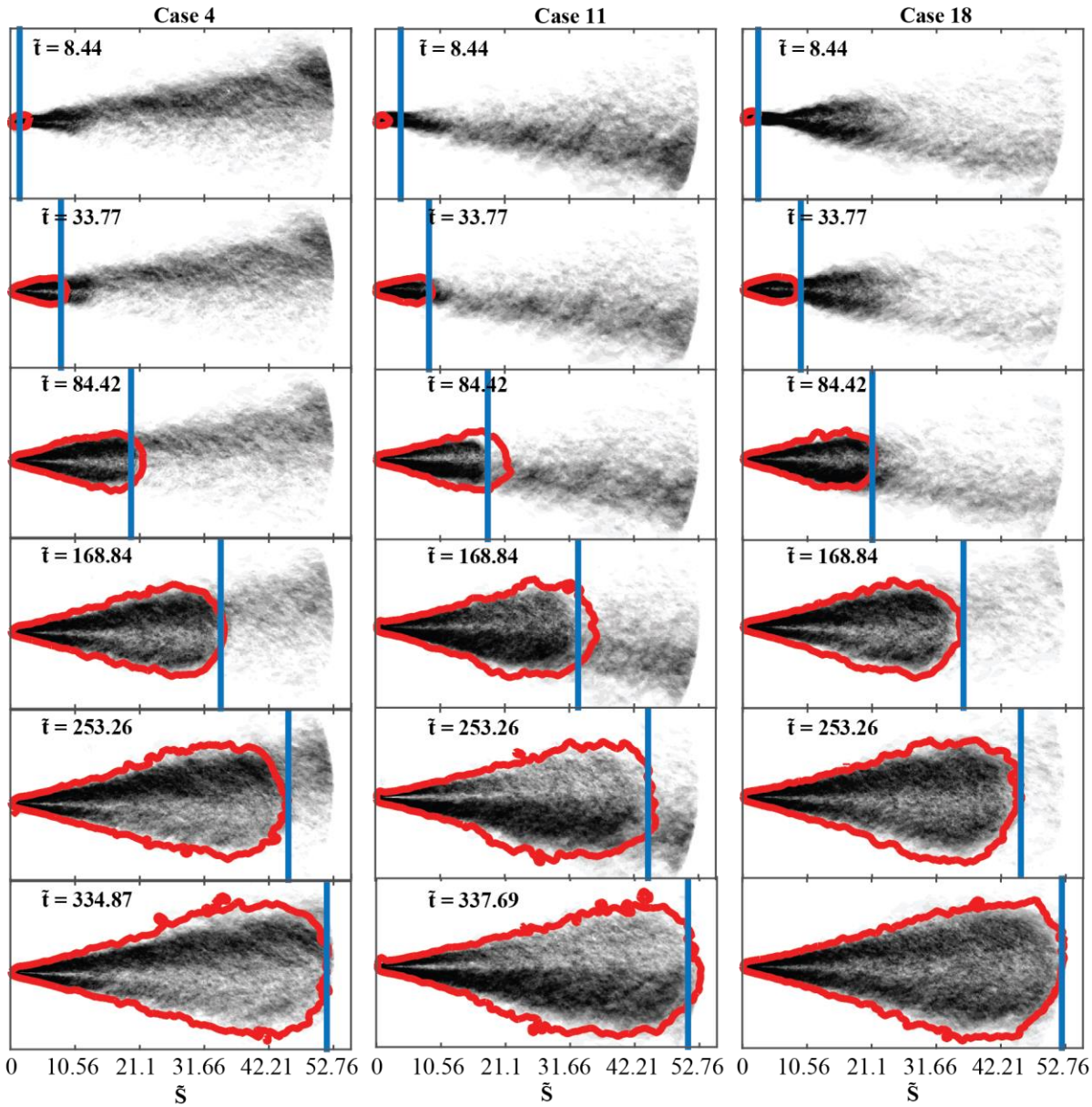

Figure 14. The sequence of schlieren images shows the relative jet-tip penetration of the first and second injection in the split injection cases (4, 11, and 18). The inverted schlieren image is the second injection fluid penetrating through the remnants of the first injection. Time is given in non-dimensional time from SOI relative to each injection, where $\tilde{t} = 0$ is SOI_1 and SOI_2. The red lines overlaid on the image represent the boundary of the first injection and the blue line represents the location of the jet tip of the second injection found using the jet tip tracking algorithm in Appendix A.

References

1. EPA, United States. 2014. Control of Air Pollution from Motor Vehicles: Tier 3 Motor Vehicle Emission and Fuel Standards. Federal Register.
2. 2009. Regulation (EC) European Parliament.
3. Tanaka, Takehiro, Ando, Akihiro, and Ishizaka, Kazuyoshi. 2002. "Study on pilot injection of DI diesel engine using common-rail injection system." *JSAE review* 23 (3):297-302.

4. Zhang, Long. 1999. A study of pilot injection in a DI diesel engine. SAE Technical Paper.
5. Busch, Stephen, Zha, Kan, Miles, Paul C, Warey, Alok, Pesce, Francesco, Peterson, Richard, and Vassallo, Alberto. 2015. "Experimental and Numerical Investigations of Close-Coupled Pilot Injections to Reduce Combustion Noise in a Small-Bore Diesel Engine." *SAE International Journal of Engines* 8 (2015-01-0796):660-678.
6. Zeng, Weilin, He, Xu, Jin, Senjia, Liu, Hai, Li, Xiangrong, and Liu, Fushui. 2013. "Analysis of the influence of pilot injection timing on diesel combustion in an optical engine by the two-color method." ASME 2013 Internal Combustion Engine Division Fall Technical Conference.
7. Bakenhus, Marco, and Reitz, Rolf D. 1999. Two-color combustion visualization of single and split injections in a single-cylinder heavy-duty DI diesel engine using an endoscope-based imaging system. SAE Technical Paper.
8. Bower, Glenn R, and Foster, David E. 1993. The effect of split injection on fuel distribution in an engine-fed combustion chamber. SAE Technical Paper.
9. Han, Zhiyu, Uludogan, All, Hampson, Gregory J, and Reitz, Rolf D. 1996. Mechanism of soot and NOx emission reduction using multiple-injection in a diesel engine. SAE Technical Paper.
10. Tow, TC, Pierpont, DA, and Reitz, Rolf D. 1994. Reducing particulate and NOx emissions by using multiple injections in a heavy duty DI diesel engine. SAE Technical Paper.
11. Nehmer, Daniel A, and Reitz, Rolf D. 1994. Measurement of the effect of injection rate and split injections on diesel engine soot and NOx emissions. SAE Technical Paper.
12. Ehleskog, Rickard, Golovitchev, Valeri, Denbratt, Ingemar, Andersson, Sven, and Rinaldini, Carlo Alberto. 2006. Experimental and numerical investigation of split injections at low load in an HDDI diesel engine equipped with a piezo injector. SAE Technical Paper.
13. Herfatmanesh, Mohammad Reza, Lu, Pin, Attar, Mohammadreza Anbari, and Zhao, Hua. 2013. "Experimental investigation into the effects of two-stage injection on fuel injection quantity, combustion and emissions in a high-speed optical common rail diesel engine." *Fuel* 109:137-147.
14. Skeen, Scott, Manin, Julien, and Pickett, Lyle M. 2015. "Visualization of Ignition Processes in High-Pressure Sprays with Multiple Injections of n-Dodecane." *SAE International Journal of Engines* 8 (2015-01-0799):696-715.
15. 2015. "Engine Combustion Network." Accessed July 15, 2015. http://www.sandia.gov/ecn/.
16. Goldwine, Gideon, and Sher, Eran. 2009. "Experimental investigation of the effect of split injection on diesel engine performance." *International Journal of Vehicle Design* 50 (1-4):66-90.
17. Herfatmanesh, Mohammad Reza, and Zhao, Hua. 2012. "Experimental investigation of effects of dwell angle on fuel injection and diesel combustion in a high-speed optical CR diesel engine." *Proceedings of the Institution of Mechanical Engineers, Part D: Journal of Automobile Engineering*:0954407012450656.
18. O'Connor, Jacqueline, and Musculus, Mark. 2013. "Optical Investigation of the Reduction of Unburned Hydrocarbons Using Close-Coupled Post Injections at LTC Conditions in a Heavy-Duty Diesel Engine." *SAE International Journal of Engines* 6 (2013-01-0910):379-399.
19. O'Connor, Jacqueline, and Musculus, Mark. 2014. "Effect of Load on Close-Coupled Post-Injection Efficacy for Soot Reduction in an Optical Heavy-Duty Diesel Research Engine." *Journal of Engineering for Gas Turbines and Power* 136. doi: 10.1115/1.4027276.
20. O'Connor, Jacqueline, and Musculus, Mark. 2014. "In-cylinder mechanisms of soot reduction by close-coupled post-injections as revealed by imaging of soot luminosity and planar laser-induced soot incandescence in a heavy-duty diesel engine." *SAE International Journal of Engines* 7 (2014-01-1255):673-693.
21. Hessel, Randy, Reitz, Rolf D, Musculus, Mark, O'Connor, Jacqueline, and Flowers, Daniel. 2014. "A CFD Study of Post Injection Influences on Soot Formation and Oxidation under Diesel-Like Operating Conditions." *SAE International Journal of Engines* 7 (2014-01-1256):694-713.
22. Yun, Hanho, Sun, Yong, and Reitz, Rolf D. 2005. "An experimental and numerical investigation on the effect of post injection strategies on combustion and emissions in the low-temperature diesel combustion regime." ASME 2005 Internal Combustion Engine Division Spring Technical Conference.
23. Bobba, Mohan, Musculus, Mark, and Neel, Wiley. 2010. "Effect of post injections on in-cylinder and exhaust soot for low-temperature combustion in a heavy-duty diesel engine." *SAE International Journal of Engines* 3 (2010-01-0612):496-516.
24. Chen, S Kevin. 2000. Simultaneous reduction of NOx and particulate emissions by using multiple injections in a small diesel engine. SAE Technical Paper.
25. Hotta, Yoshihiro, Inayoshi, Minaji, Nakakita, Kiyomi, Fujiwara, Kiyoshi, and Sakata, Ichiro. 2005. Achieving lower exhaust emissions and better performance in an HSDI diesel engine with multiple injection. SAE Technical Paper.
26. Vanegas, A, Won, H, Felsch, C, Gauding, M, and Peters, N. 2008. Experimental investigation of the effect of multiple injections on pollutant formation in a common-rail DI diesel engine. SAE Technical Paper.
27. Parrish, Scott E, Zhang, Gaoming, and Zink, Ronald J. 2012. Liquid and vapor envelopes of sprays from a multi-hole fuel injector operating under closely-spaced double-injection conditions. SAE Technical Paper.
28. Bruneaux, Gilles, and Maligne, David. 2009. "Study of the mixing and combustion processes of consecutive short double diesel injections." *SAE international journal of engines* 2 (2009-01-1352):1151-1169.
29. Skeen, Scott A, Manin, Julien, and Pickett, Lyle M. 2014. Advanced Diagnostics for High Pressure Spray Combustion. Sandia National Laboratories (SNL-CA), Livermore, CA (United States).
30. Zha, Kan, Busch, Stephen, Miles, Paul C, Wijeyakulasuriya, Sameera, Mitra, Saurav, and Senecal, PK. 2015. "Characterization of Flow Asymmetry During the Compression Stroke Using Swirl-Plane PIV in a Light-Duty Optical Diesel Engine with the Re-entrant Piston Bowl Geometry." *SAE International Journal of Engines* 8 (2015-01-1699).
31. Jung, Yongjin, Manin, Julien, Skeen, Scott, and Pickett, Lyle M. 2015. Measurement of Liquid and Vapor Penetration of Diesel Sprays with a Variation in Spreading Angle. SAE Technical Paper.
32. Eagle, W. Ethan, Musculus, Mark P. B., Malbec, L-M. C. , and Bruneaux, G. 2015. "Measuring transient entrainment rates of a confined vaporizing diesel jet." ILASS Americas 26th

Annual Conference on Liquid Atomization and Spray Systems, Portland, OR.
33. Naber, Jeffrey, and Siebers, Dennis L. 1996. Effects of gas density and vaporization on penetration and dispersion of diesel sprays. SAE technical paper.
34. Abani, Neerav, and Ghandhi, Jaal B. 2012. "Behavior of Unsteady Turbulent Starting Round Jets." *Journal of Fluids Engineering* 134 (6):061202.
35. Musculus, Mark PB, and Kattke, Kyle. 2009. "Entrainment waves in diesel jets." *SAE International Journal of Engines* 2 (2009-01-1355):1170-1193.
36. Han, Donghee, and Mungal, MG. 2001. "Direct measurement of entrainment in reacting/nonreacting turbulent jets." *Combustion and flame* 124 (3):370-386.
37. Wakuri, Yutaro, Fujii, Masaru, Amitani, Tatsuo, and Tsuneya, Reijiro. 1960. "Studies on the penetration of fuel spray in a diesel engine." *Bulletin of JSME* 3 (9):123-130.

Contact Information

For more information, please contact the corresponding author, Meghan Borz, at meg.j.borz@gmail.com.

Acknowledgments

The authors wish to acknowledge the support of this work provided by Volvo Technology of America and the U.S. Department of Energy under DOE award number DEEE0004232. Thanks to Samuel Mclaughlin and Richard Morton of Volvo Technology of America. Additionally, the authors thank Daniel Ruth for his assistance with image post-processing.

Definitions/Abbreviations

a	0.66, experimentally determined coefficient from [33] that relates the angle of the model equations to the measured angle for non-vaporizing sprays
BTDC	Before top dead center
Ca	Area contraction coefficient
CNL	Combustion noise level
d_f	Effective orifice diameter
d_o	Actual orifice diameter
DOI	Duration of injection
DOI_1	Duration of first injection
DOI_2	Duration of second injection
DPF	Diesel particulate filters
ECN	Engine Combustion Network
EGR	Exhaust gas recirculation
EOI	End of injection
fps	Frames per second
HRR	Heat release rate
IMEP	Indicated mean effective pressure
LIEF	Laser induced exciplex fluorescence
NOx	Mono-nitrogen oxides
PLIF	Planar laser induced fluorescence
PM	Particulate matter
S	Jet-tip penetration
SCR	Selective catalytic reduction (exhaust aftertreatment)
SOI	Start of injection
SOI_1	Start of the first injection
SOI_2	Start of the second injection
PIV	Particle image velocimetry
TDC	Top dead center
UHC	Unburned hydrocarbons
U_f	Nozzle exit velocity
$\tilde{\rho}, \rho_a, \rho_f$	Density ratio, ambient density, and fuel density
$\theta, \theta_1, \theta_2$	Dispersion angle, dispersion angle for first injection, dispersion angle for second injection

Appendix A

The gas jet images were processed in MATLAB to determine the jet-tip penetration and spreading angle. The second injection images require a more rigorous image processing method for finding the jet-tip penetration due to increased background noise from the first injection and excess fluid. Initially, these images were processed in the same manner as the gas jet images for the first injection, but the binary images revealed that the actual jet tip was not tracked due to noise from excess fluid that leaves a jet between injections as a result of buoyancy. Because the excess fluid was subtracted from the images in the background subtraction step and was nearly the same intensity as the second injection gas jet, the background subtraction left a gap in the center of the second jet, as shown in Figure 15.

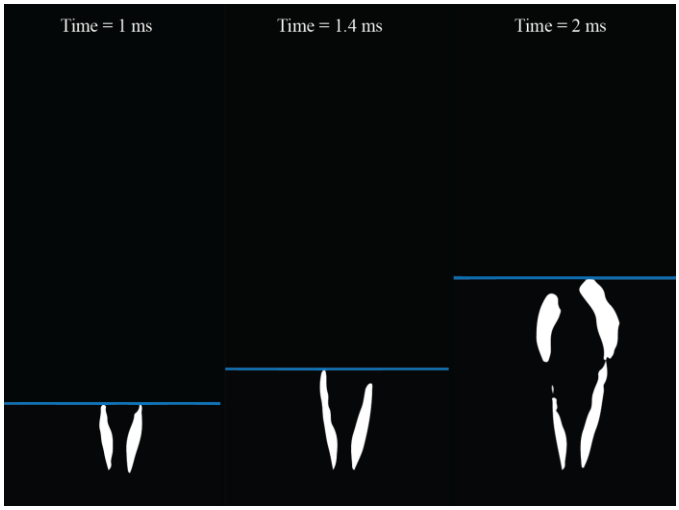

Figure 15. Binary images at three instances in time after SOI_2 are shown for case 15. The excess fluid following the first injection was subtracted during the background subtraction step of image processing. The intensity of the excess fluid was the same as the intensity of the second injection gas jet, resulting in the tip of the second injection gas jet being subtracted out in the near-nozzle region. The location of the jet tip as determined by the original algorithm is represented by the blue line.

To mitigate these issues, a sliding background subtraction technique is utilized and the region with the highest intensity gradient is used to determine the location of the jet tip. First, the start of the injection is determined using the pressure measurements taken inside of the injector cavity. This method was validated using visual inspection of the first injection images, which showed that the start of the gas jet could be seen within 1-2 frames of the time where the pressure first rose. Thirty images prior to the frame for SOI_1 are averaged and subtracted from the injection images in the pre-background subtraction step. The absolute value of the image is taken to account for the negative intensity on one side of the jet and the positive intensity on the opposite side of the jet (resulting from using a vertical knife edge) following the pre-background subtraction step. A sliding background technique has also been reported by Skeen *et al*. [14] for use in multiple diesel injections.

The sliding background subtracted images are obtained by averaging three pre-background subtracted images following the image of interest (i+1, i+2, and i+3) and subtracting the image of interest (i^{th} image) from the averaged image as shown in Figure 15a. Next, the image is binarized using a threshold of 0.08 for the first 15 frames and a threshold of 0.1 for all following frames. The function ‘bwareaopen’ was used to reduce noise by eliminating all open areas that were smaller than 350 pixels as shown in Figure 15b. To evaluate the intensity at each downstream location, pixel intensity is averaged over 30 columns (around the centerline) and 5 rows (the row of interest and two rows above and below it). The gradient of the intensity averaged matrix is found using the diff function, which calculates the difference between adjacent elements. The maximum gradient is found at each instant in time, which provides the downstream location where the image transitions from the dark region where the jet is located to the white region where the jet will be in the next three frames, as shown in figure 15d.

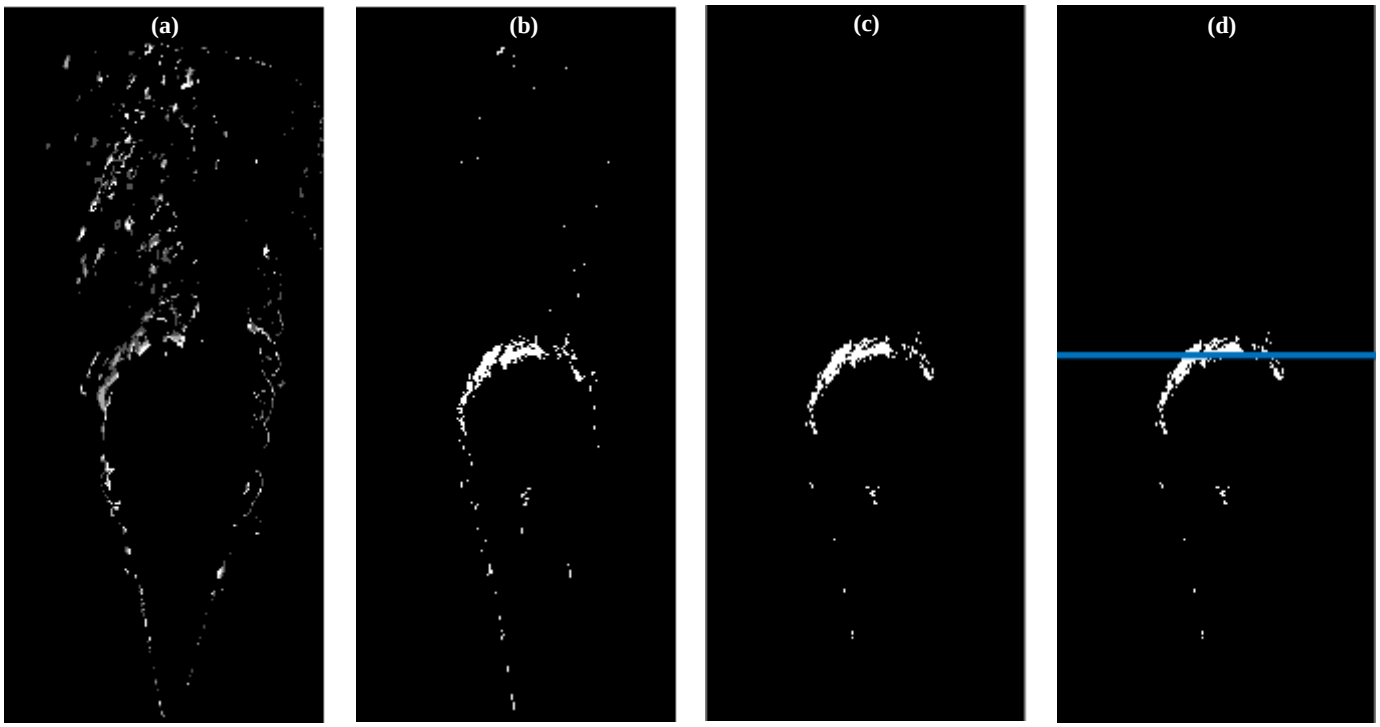

Figure 16. Images for case 15 at 3.067 ms after SOI_2 are shown after the following processing steps: (a) subtracting i^{th} background subtracted image from the average of i+1, i+2, and i+3 images, (b) binarization with a 0.1 threshold, (c) binarization with noise reduction, and (d) determination of the location of highest intensity gradient represented by the blue line.

However, near SOI_2, there is a significant amount of noise in the region of the images where the jet tip is located. Oftentimes, a region that does not correspond to the location of the actual jet tip is the region with the highest intensity gradient. The algorithm was improved by limiting the search region. This is achieved by fitting a rational or polynomial curve (determined on a case-by-case basis using the cftool) to the points later in time on the penetration plot, which accurately track the jet tip, and placing upper and lower bounds +/- 30 pixels above and below the curve as shown in Figure 17. The jet tip location near SOI_2 is the location of the highest intensity gradient that does not vary more than 5 pixels above or below the previously found point and is within the search bounds. If the data point with the highest intensity gradient is not within 5 pixels of the jet tip location found before it, the algorithm finds the next highest intensity gradient. The search process for one point iterates until the search criteria is met or 5 iterations have occurred. If the jet tip location has not been found after 5 iterations, the point is thrown out because there is too much noise in the image to accurately find the jet tip.

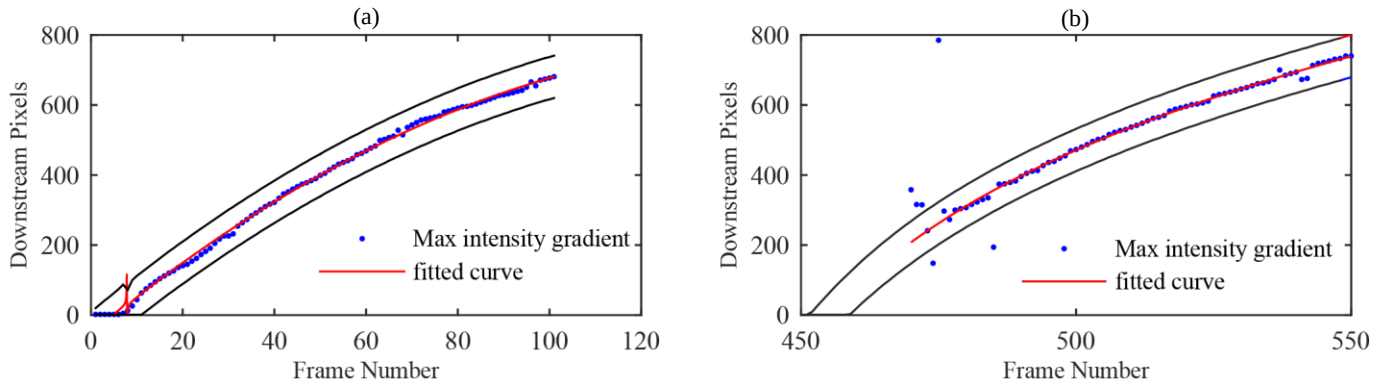

Figure 17. The search bounds for case 15 were found by fitting a rational curve to data that followed the jet tip later in the injection. The concept for finding the search bounds was proven on the first injection (a) and repeated for the second injection (b).